

IEEE 802.11ac/ax: Lessons Learned on OFDM MU-MIMO Transceivers with Realistic Feedback over TGac Channels with Doppler Spread

Roger Pierre Fabris Hoefel

Electrical Engineering Department
Federal University of Rio Grande do Sul (UFRGS)
Porto Alegre, RS, Brazil
roger.hoefel@ufrgs.br

Abstract— In this paper, we investigate the effects of channel state information (CSI) compression and feedback delay on the downlink (DL) performance of multi-user multiple input multiple output (MU-MIMO) IEEE 802.11ac systems over dynamic TGac channels with Doppler spread. We show that using degrees of freedom available at receiver side to cancel the MU interference decreases the detrimental effects of CSI imperfections on the performance of 802.11ac wireless local area networks. Fundamentally, we have concluded that iterative real time radio resource algorithms are fundamental to optimize the system configuration since the performance of 802.11ac DL MU-MIMO transceivers depends on a multitude of systems parameters and dynamic random variables.

Keywords—802.11ac, MU-MIMO, Channel State Information.

I. INTRODUCTION

The IEEE 802.11ac amendment was approved at late 2013 [1]. In one hand, the Wireless Fidelity (Wi-Fi) semiconductor players continue developing research and design (R&D) activities to improve the performance of 802.11ac second wave products, such as, implementation of downlink multi-user multiple input multiple output (DL MU-MIMO) techniques; bandwidths (BW) of 80 and 160 MHz; four spatial streams (SS) and 256 quadrature amplitude modulation (256-QAM). This allows a maximum physical layer (PHY) throughput of ~ 3.5 Gbps, while the maximum specified PHY throughput is ~ 7 Gbps, assuming 256-QAM, 8 SS and 160 MHz BW [2, pp. 213]. On the other hand, the Task Group (TG) 802.11ax was created in April 2014 to develop a new 802.11 amendment to face with the challenges of exponential increase of traffic and number of devices in dense networks and Internet of Things (IoT); competition of Long Term Evolution Unlicensed (LTE-U) to offload traffic; pressure of chip set vendors to create a Wi-Fi market after the 802.11ac amendment [3]. Therefore, R&D activities on the effects of realistic feedback schemes on the performance of MU-MIMO transceivers have importance in short and long terms.

The remaining of this paper is organized as follows: Section II presents our main motivations and related works. Section III describes main aspects related to the design DL MU-MIMO transceivers in 802.11ac systems. Section IV presents a consistent set of simulation results in order to investigate the effects of realistic channel state information (CSI) feedback

schemes on the performance of IEEE 802.11ac wireless local area network (WLANs) assuming dynamic spatial-correlated frequency selective MU-MIMO TGac channels. Finally, our conclusions are stated in Section V.

II. MOTIVATIONS AND RELATED WORK

Many papers that have investigated the performance of DL MU-MIMO transceivers assume perfect CSI information at both transmitter (TX) and receiver (RX) sides. For instance, it is shown in [4] that the implementation of an adaptive receiver that switches between interference whitening and interference MIMO detection allows complexity reduction with controllable performance degradation with relation to (w.r.t.) the maximum likelihood (ML) MIMO detector. However, the challenges of feedback delay and CSI compression were not fully investigated in [4]. In [5], it was carried out a performance evaluation of the DL MU-MIMO 802.11ac systems that implement the following channel sounding techniques: explicit (assuming compressed Givens rotation feedback scheme); implicit (considering calibration errors). The simulation results show that a non-standardized hybrid implicit technique has a better performance w.r.t. the explicit technique specified in 802.11ac amendment [1,2]. However, the Doppler effects were not analyzed and only stations (STAs) with one antenna (i.e., low-tier devices) were assumed in [5]. In [6], the performance of 802.11ac transceivers with either channel inversion (CI) precoder or block diagonalization (BD) precoder and zero forcing (ZF) MIMO detector were studied in order to assess the performance of user selection algorithms. In [7], it was investigated the performance of generalized sphere decoding (GSD) MIMO detectors in the framework of 802.11ac DL MU-MIMO. Although, the references [6] and [7] only shown simulation results using CSI feedback scheme based on Givens rotation compression with $(\psi, \phi) = (5, 7)$ bits [7] and $(\psi, \phi) = (7, 9)$ bits [6,7] over channels without Doppler spread. In this paper, we shall investigate the effects of different levels of quantization on the performance of 802.11ac systems with regularized channel inversion minimum mean squared error (RI-MMSE) precoder and interference cancellation (IC) MMSE MIMO detectors, assuming dynamic spatial-correlated frequency TGac MU-MIMO channels.

In this contribution, we also show that the equivalent MU-

MIMO channel matrix available at TX side to calculate the precoder is different from the usual mathematical model used for the DL MU-MIMO channel matrix due to the characteristics of the feedback scheme specified in the IEEE 802.11ac amendment. Therefore, we carry out a performance comparison between the 802.11ac transceivers with precoders that use the DL MU-MIMO channel matrix and transceivers with precoders that use the 802.11ac equivalent DL MU-MIMO channel matrix. We also show that using degrees of freedom (DoF) to cancel the MU interference at RX become the system performance less susceptible to the negative effects of delay and compression in the CSI feedback.

III. DOWNLINK MU-MIMO: TRANSCEIVER DESIGN

Signal processing operations are performed per subcarrier in MIMO Orthogonal Frequency Division Multiplexing (OFDM) PHY. In order to simplify the notation, we omit the index that specifies the subcarrier being processed when this can be perfectly inferred from the context.

A. Received Signal Model For DL MU-MIMO Channel

The received symbols in the frequency domain for the DL MU-MIMO OFDM channel with K users can be modeled as follows:

$$\mathbf{y} = \begin{bmatrix} \mathbf{y}_1 \\ \mathbf{y}_2 \\ \vdots \\ \mathbf{y}_K \end{bmatrix} = \mathbf{H}_{DL}\mathbf{x} + \mathbf{z} = \begin{bmatrix} \mathbf{H}_1 \\ \mathbf{H}_2 \\ \vdots \\ \mathbf{H}_K \end{bmatrix} \cdot [x_1, x_2, \dots, x_{n_t}]^T + \begin{bmatrix} \mathbf{z}_1 \\ \mathbf{z}_2 \\ \vdots \\ \mathbf{z}_K \end{bmatrix}, \quad (1)$$

where the DL MU-MIMO channel is given by the matrix \mathbf{H}_{DL} with size $n_{r,total} = \sum_{u=1}^K n_{r,u}$ by n_t , where $n_{r,u}$ is the number of receive antennas of the u th station (STA) and n_t is the number of transmit antennas at the access point (AP). The matrix \mathbf{H}_u , with size $n_{r,u}$ by n_t , models the DL MIMO channel matrix observed by the u th user [8, pp. 401].

The received signal by the u th user is given by

$$\mathbf{y}_u = \mathbf{H}_u\mathbf{x} + \mathbf{z}_u, \quad u = 1, \dots, K. \quad (2)$$

The column vector \mathbf{z} in (1) models the zero mean circular symmetric complex Gaussian (ZMCSCG) noise. This vector is formed by K random vectors, where each column vector $\mathbf{z}_u = [z_{u,1}, z_{u,2}, \dots, z_{u,n_{r,u}}]^T, u = 1, \dots, K$, is composed by $z_{u,j} (j = 1, \dots, n_{r,u})$ independent and identical distributed (i.i.d.) ZMCSCG random variables (r.v.) with equal variance N_0 .

The symbols at the output of the transmit antenna elements are given by $\mathbf{x} = \mathbf{P} \cdot \mathbf{s}$, where \mathbf{P} is the precoding matrix with size n_t by $n_{ss,total} = \sum_{u=1}^K n_{ss,u}$, where $n_{ss,u}$ and $n_{ss,total}$ denote, respectively, the number of SS transmitted to the u th STA and the total number of SS transmitted to all K STAs. The transmitted symbols for all K users are modeled by the column vector $\mathbf{s} = [\mathbf{s}_{u,1}^T, \mathbf{s}_{u,2}^T, \dots, \mathbf{s}_{u,K}^T]^T$, where the symbols transmitted to the u th STA are given by the column vector $\mathbf{s}_u = [s_{u,1}, s_{u,2}, \dots, s_{u,n_{ss,u}}]^T$. The DL transmitted symbol to the u th user at j th SS is denoted by $s_{u,j}$.

B. IEEE 802.11ac Channel Sounding Mechanism

The implementation of single user (SU) MIMO adaptive transmit beamforming (TxBF) and DL MU-MIMO in 802.11ac systems needs mechanisms to sound the channel in order to obtain the CSI at TX side. The 802.11ac amendment specifies only one sounding mechanism, which it is based on the transmission of non-data-packet (NDP) by the beamformer, as shown in Fig. 1 [2, pp. 438]. The beamformees feed back the CSI using the *Compressed Beamforming Frame (CBF)*.

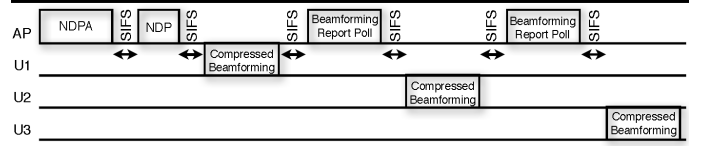


Figure 1. MU-MIMO sounding scheme used in 802.11ac. SIFS means Short InterFrame Spacing.

The explicit compressed feedback scheme specified in the IEEE 802.11ac amendment is based on the singular value decomposition (SVD) of the MIMO channel matrix observed at each STA involved in the sounding procedure, i.e.,

$$\mathbf{H}_u = \mathbf{U}_u \mathbf{S}_u \mathbf{V}_u^H = \mathbf{U}_u [\mathbf{S}_u^{\text{non-zero}} \mathbf{0}] \begin{bmatrix} (\mathbf{V}_u^{\text{non-zero}})^H \\ (\mathbf{V}_u^{\text{zero}})^H \end{bmatrix}. \quad (3)$$

Notice that the matrix \mathbf{H}_u that is fed back by u th STA during the sounding procedure has size $n_{ss,u}$ by n_t , i.e., the rank depends on the user selection scheduling algorithm that specifies the channel dimensionality to be sounded. However, during the phase of data transmission, the channel matrix has size $n_{r,u}$ by n_t , since all RX antennas must be used in the MIMO detection algorithm to improve the system performance due to diversity gain and/or interference cancellation.

The matrix $\mathbf{U}_u \in \mathbb{C}^{n_{ss,u} \times n_{ss,u}}$ has the left singular vectors of matrix \mathbf{H}_u . The matrix of singular values of \mathbf{H}_u is denoted by $\mathbf{S}_u \in \mathbb{C}^{n_{ss,u} \times n_t}$, where the matrix that contains only the non-zero singular values is denoted by $\mathbf{S}_u^{\text{non-zero}} \in \mathbb{C}^{n_{ss,u} \times n_{ss,u}}$. The matrix of all zeros $\mathbf{0}$ has size $n_{ss,u}$ by $n_t - n_{ss,u}$. The superscript $(\cdot)^H$ denotes the Hermitian transpose operator.

The matrix $\mathbf{V}_u \in \mathbb{C}^{n_t \times n_t}$ is formed by the right singular vectors of the matrix \mathbf{H}_u . The matrices $\mathbf{V}_u^{\text{non-zero}} \in \mathbb{C}^{n_t \times n_{ss,u}}$ and $\mathbf{V}_u^{\text{zero}} \in \mathbb{C}^{n_t \times (n_t - n_{ss,u})}$ contain the right singular vectors that correspond to the non-zero and zero singular values, respectively, of the matrix \mathbf{H}_u . $\mathbf{V}_u^{\text{zero}}$ is an orthonormal basis for the null space of \mathbf{H}_u .

The IEEE 802.11ac amendment specifies that each user involved in the sounding procedure must implement an algorithm based on Givens Rotation to compress the $\mathbf{V}_u^{\text{non-zero}}$ matrix in the form of two sets of angles. This information is transmitted in the *Compressed Beamforming Report field* of the *CBF*, as described in the next subsection.

When the transceiver is engaged in DL MU-MIMO, the *CBF* also contains the *MU Exclusive Beamforming Report field*, where the average signal-to-noise ratio (SNR) per SS and $SNR_{i,k}$ of the k th subcarrier (SC) at the i th SS are transmitted.

The proprietary MIMO channel estimation scheme implemented at 802.11ac RX must use the pilots of the very-high throughput long training field (VHT-LTF) transmitted in the preamble of NDP and data packets [2, pp. 195]. Since the Hadamart cover matrix used to transmit the pilots in the VHT-LTF is orthogonal, then the average SNR can be estimated using classical techniques designed for OFDM systems [9]. Observe that the average SNR is practically the same for each SS. The $SNR_{i,k}$, assuming that the transceiver implements a precoder based on SVD and MMSE MIMO detector, is given by [2, pp. 371]

$$SNR_{i,k} = \frac{1/n_t}{N_0} \frac{1}{\text{diag}_i \left\{ \left[\left(\mathbf{H}_u^{(k)} \mathbf{V}_u^{\text{non-zero}(k)} \right)^H \mathbf{H}_u^{(k)} \mathbf{V}_u^{\text{non-zero}(k)} \right]^{-1} \right\}}$$

$$SNR_{i,k} = \overline{SNR} \cdot S_{i,k}^2, \quad (4)$$

where it is assumed the transmitted power is normalized. Notice that in (4), for completeness, it was included the subscript (k) that indicates the k th subcarrier being processed.

Finally, the beamformer can build the channel equivalent matrix using the information transported by the CABF (i.e., compressed $\mathbf{V}_u^{\text{non-zero}}$, \overline{SNR} and $SNR_{i,k}$), i.e.,

$$\mathbf{H}_{EQ} = \begin{bmatrix} \mathbf{S}_1^{\text{non-zero}} (\mathbf{V}_1^{\text{non-zero}})^H \\ \mathbf{S}_2^{\text{non-zero}} (\mathbf{V}_2^{\text{non-zero}})^H \\ \vdots \\ \mathbf{S}_K^{\text{non-zero}} (\mathbf{V}_K^{\text{non-zero}})^H \end{bmatrix}. \quad (5)$$

The matrix \mathbf{H}_{EQ} is the one effectively used at the TX to calculate the precoding matrix when the technical details of the IEEE 802.11ac sounding procedure are taken into account, i.e., the real-world scenario. Note that the matrix \mathbf{U}_u is not present in (5). However, the information contained in this matrix is incorporated in the effective MIMO channel matrix estimated by the u th STA, which it is necessary to calculate the MIMO detector. Observe that the VHT-LTF are precoded by the matrix \mathbf{P} when the medium access control packet data units (MPDU), which can contain data and/or control information, are transmitted from the beamformer to the beamformees.

C. 802.11ac Compression: Givens Planar Rotation

The matrix $\mathbf{V}_u^{\text{non-zero}}$, originated from applying the SVD in the MIMO channel matrix observed by the u th, is *unitary*, i.e., $(\mathbf{V}_u^{\text{non-zero}})^H \mathbf{V}_u^{\text{non-zero}} = \mathbf{V}_u^{\text{non-zero}} (\mathbf{V}_u^{\text{non-zero}})^H = \mathbf{I}$. The use of Givens rotation allows representing unitary matrices using angles of polar coordinates, and, consequently, the number of bits necessary to represent unitary matrices can be compressed. For instance, assuming a full rank 2×2 MIMO channel matrix \mathbf{H} , then the matrix $\mathbf{V} = \mathbf{V}^{\text{non-zero}}$ can be expressed as

$$\mathbf{V} = \begin{bmatrix} \cos(\psi_1) \cdot e^{j\theta_1} & \cos(\psi_2) \cdot e^{j\theta_2} \\ \sin(\psi_1) & \sin(\psi_2) \end{bmatrix} = \begin{bmatrix} e^{j\theta_1} & 0 \\ 0 & 1 \end{bmatrix} \begin{bmatrix} \cos(\psi_1) & -\sin(\psi_1) \\ \sin(\psi_1) & \cos(\psi_1) \end{bmatrix}, \quad (6)$$

when the following conditions are accomplished: (i) $\psi_1 -$

$\psi_2 = \pi/2$ and $\theta_1 = \theta_2$ or (ii) $\psi_1 + \psi_2 = \pi/2$ and $\theta_1 = \theta_2 + \pi$. Hence, $\psi \in [0, \pi/2)$ and $\phi \in [0, 2\pi)$. In summary, in this example it is only necessary to have the angles ψ and θ to rebuild the matrix \mathbf{V} with rank 2. In the following, we shall describe fundamental topics on application of Givens rotation technique to compress the CSI in 802.11ac systems [1], [2, pp. 388]. The objective is to summarize the minimal information necessary to understand the issues related to the compression scheme that has been adopted in the IEEE 802.11 framework.

The unitary matrix $\mathbf{V}_u^{\text{non-zero}}$ originated from applying SVD in MIMO channel matrix observed by the u th STA is given by (7), where $\tilde{\mathbf{I}}_{n_t \times n_{ssu}}$ is an modified unitary matrix with size $n_t \times n_{ssu}$ with extra rows or columns composed with zeros when $n_t \neq n_{ssu}$ [2, pp. 389].

$$\mathbf{V}_u^{\text{non-zero}} = \left(\prod_{i=1}^{\min(n_t, n_{ssu})} [\mathbf{D}_i \prod_{j=i+1}^{n_t} \mathbf{G}_{ji}(\psi_{j,i})] \times \tilde{\mathbf{I}}_{n_t \times n_{ssu}} \right) \tilde{\mathbf{D}}. \quad (7)$$

The Givens planar rotation operates over real numbers, but the unitary matrix $\mathbf{V}_u^{\text{non-zero}}$ belongs to the complex field. Therefore, it is necessary to use the matrices \mathbf{D}_i and $\tilde{\mathbf{D}}$ as follows: the diagonal matrix $\tilde{\mathbf{D}}$ with size $n_{ssu} \times n_{ssu}$ has its main diagonal elements given by $\{e^{j\theta_i}, i = 1, \dots, n_{ssu}\}$, such as the *last row* of the matrix $\mathbf{V}_u^{\text{non-zero}} \tilde{\mathbf{D}}^H$ contains only non-negative real values. These angles are given by $\theta_i = \text{angle}(\mathbf{V}_u^{\text{non-zero}} \tilde{\mathbf{D}}^H)_{n_t, i}$, i.e., these angles depends on the complex elements of the *last row* of the matrix $\mathbf{V}_u^{\text{non-zero}}$.

The diagonal matrix \mathbf{D}_i is given by

$$\mathbf{D}_i = \begin{bmatrix} \mathbf{I}_{i-1} & 0 & \dots & \dots & 0 \\ 0 & e^{j\phi_{i,i}} & 0 & \dots & 0 \\ \vdots & 0 & \ddots & 0 & \vdots \\ \vdots & \vdots & 0 & e^{j\phi_{n_t-1,i}} & 0 \\ 0 & 0 & \dots & 0 & 1 \end{bmatrix}. \quad (8)$$

The angles of the matrix \mathbf{D}_1 , $\{\phi_{j,1}, j = 1, \dots, n_{ssu} - 1\}$ are obtained such as all elements of first column of $\mathbf{D}_1^H (\mathbf{V}_u^{\text{non-zero}} \tilde{\mathbf{D}}^H)$ are all non-negative real numbers, i.e., $\phi_{j,1} = \text{angle}(\mathbf{V}_{j,1}^{\text{non-zero}})$. Observe that the matrix \mathbf{D}_1^H does not change the last row of matrix $\mathbf{V}_u^{\text{non-zero}}$ since the last element of its diagonal principal is one. Therefore, this is the reasoning why the matrix $\mathbf{V}_u^{\text{non-zero}}$ must be right-multiplied by the matrix $\tilde{\mathbf{D}}^H$, as described in the previous paragraph. The reader is referenced to [1-2] to obtain a clearly explanation of the procedures necessary to calculate all the set of angles ϕ to build the remaining matrices $\mathbf{D}_i, i = 2, \dots, \min(n_t, n_{ssu})$.

The Givens matrix is given by (9), where \mathbf{I}_n denotes the identity matrix with size n and the term $\cos(\psi_{j,i})$ is located at j th row and i th column.

$$\mathbf{G}_{ji}(\psi) = \begin{bmatrix} \mathbf{I}_{i-1} & 0 & 0 & 0 & 0 \\ 0 & \cos(\psi_{j,i}) & 0 & \sin(\psi_{j,i}) & 0 \\ 0 & 0 & \mathbf{I}_{j-i-1} & 0 & 0 \\ 0 & -\sin(\psi_{j,i}) & 0 & \cos(\psi_{j,i}) & 0 \\ 0 & 0 & 0 & 0 & \mathbf{I}_{n_t-1} \end{bmatrix}. \quad (9)$$

The coefficients of each Given matrix are obtained by solving the following problem [2, pp. 388]:

$$\begin{bmatrix} \cos(\psi) & \sin(\psi) \\ -\sin(\psi) & \cos(\psi) \end{bmatrix} \begin{bmatrix} x_1 \\ x_2 \end{bmatrix} = \begin{bmatrix} y \\ 0 \end{bmatrix} = \begin{bmatrix} \sqrt{x_1^2 + x_2^2} \\ 0 \end{bmatrix}, \quad (10)$$

where x_1 and x_2 denote the *real values* from the matrix where the planar rotation is being performed. The solution of (10) is given by

$$\psi = \cos^{-1}\left(\frac{x_1}{\sqrt{x_1^2 + x_2^2}}\right) = \sin^{-1}\left(\frac{x_2}{\sqrt{x_1^2 + x_2^2}}\right). \quad (11)$$

Notice that the matrix $\mathbf{G}_{21}(\psi)$ is obtained by setting x_1 and x_2 in (10) equal to the elements $[\mathbf{D}_1^H \mathbf{V}_u^{\text{non-zero}} \tilde{\mathbf{D}}^H]_{1,1}$ and $[\mathbf{D}_1^H \mathbf{V}_u^{\text{non-zero}} \tilde{\mathbf{D}}^H]_{2,1}$, respectively. The reader is referenced to [1-2] to obtain a readable description of how to build all the Givens matrices $\mathbf{G}_{ji}(\psi)$ necessary to calculate all the set of angles ψ .

The set of angles that must be feed back to obtain the matrix $\mathbf{V}_u^{\text{non-zero}}$ using (7) are given in [1]. For example, for a typical configuration with four transmit antennas and two receive antennas, each STA must feed back the following angles:

$$\{\phi_{1,1}, \phi_{2,1}, \phi_{3,1}, \psi_{2,1}, \psi_{3,1}, \psi_{4,1}, \phi_{2,2}, \phi_{3,2}, \psi_{3,2}, \psi_{4,2}, \phi_{3,3}, \psi_{4,3}\}, \quad (12)$$

Observe that the angles $\{\theta_i, i = 1, \dots, n_{ss,u}\}$ used to build the matrix $\tilde{\mathbf{D}}$ are not fed back. Hence, the TX can only rebuild the matrix $\mathbf{V}_u^{\text{non-zero}} \tilde{\mathbf{D}}^H$. However, using this approximate matrix does not change the observable SNR at RX side [2, pp. 389].

The angles ϕ and ψ are uniformed quantized in the intervals $[0, 2\pi)$ and $[0, \pi/2)$, respectively, as follows:

$$\begin{cases} \phi = \frac{\pi}{2^{b+1}} + \frac{k\pi}{2^{b+2}}, & k = 0, \dots, 2^{b+2} - 1 \\ \psi = \frac{\pi}{2^{b+1}} + \frac{k\pi}{2^{b+2}}, & k = 0, \dots, 2^b - 1 \end{cases}, \quad (13)$$

where $(b+2)$ and (b) are number of bits to quantize the angles ϕ and ψ , respectively. Note that (b) can be 1, 2, 3 or 4 [2, pp. 392].

D. MU-MIMO Precoding

The regularized channel inversion minimum mean squared error (RI-MMSE) precoding matrix, considering that all STAs have the same average SNR, is given by [10]

$$\mathbf{P}_{MMSE} = \beta_{MMSE} \cdot \mathbf{H}_{DL}^H \cdot \left[\mathbf{H}_{DL} \cdot \mathbf{H}_{DL}^H + \frac{1}{\text{SNR}} \mathbf{I}_{n_{ss,total}} \right]^{-1}, \quad (14)$$

where $\mathbf{I}_{n_{ss,total}}$ denotes a diagonal matrix with dimension $n_{ss,total}$ and the normalization factor of the transmitted power is given by

$$\beta_{MMSE} = \sqrt{\frac{n_t}{\text{trace}(\mathbf{P}_{MMSE} \cdot \mathbf{P}_{MMSE}^H)}}. \quad (15)$$

The feedback scheme specified in the 802.11ac amendment, as earlier described, does not allow that the TX rebuild the MU-MIMO channel matrix \mathbf{H}_u for each one of the K users. Therefore, the equivalent channel matrix \mathbf{H}_{EQ} given by (5) must replace \mathbf{H}_{DL} in (14) when the real world concerns are in vogue.

E. MMSE And IC-MMSE MU-MIMO Detectors

The received signal vector at the output of the MIMO detector for the u th STA can be modeled as

$$\tilde{\mathbf{y}}_u = \mathbf{W}_u^H \mathbf{y}_u = \mathbf{W}_u^H \cdot (\mathbf{H}_u \mathbf{P} \mathbf{s} + \mathbf{z}_u), \quad (16)$$

where the received signal for the u th STA is given by (2) and the matrix \mathbf{W}_u , with size $n_{r,u}$ by $n_{ss,u}$, denotes the linear MIMO detector for the u th STA.

Eq. (15) can be rewritten as

$$\tilde{\mathbf{y}}_u = \mathbf{W}_u^H \cdot (\mathbf{H}_u \mathbf{P}_1 \mathbf{s}_1 + \dots + \mathbf{H}_u \mathbf{P}_u \mathbf{s}_u + \dots + \mathbf{H}_u \mathbf{P}_K \mathbf{s}_K + \mathbf{z}_u), \quad (17)$$

where \mathbf{P}_u , with dimension n_t by $n_{ss,u}$, denotes the columns of the matrix \mathbf{P} used to precoding the symbols transmitted to the u th STA. Denoting the effective channel matrix observed by u th user as $\tilde{\mathbf{H}}_u = \mathbf{H}_u \mathbf{P}$, i.e.,

$$\tilde{\mathbf{H}}_u = [\mathbf{H}_u \mathbf{P}_1, \dots, \mathbf{H}_u \mathbf{P}_u, \dots, \mathbf{H}_u \mathbf{P}_K] = [\tilde{\mathbf{H}}_{u,1}, \dots, \tilde{\mathbf{H}}_{u,u}, \dots, \tilde{\mathbf{H}}_{u,K}]. \quad (18)$$

then (16) and (17) can be conveniently rewritten as (19) and (20), respectively.

$$\tilde{\mathbf{y}}_u = \mathbf{W}_u^H \cdot (\tilde{\mathbf{H}}_u \mathbf{s} + \mathbf{z}_u). \quad (19)$$

$$\tilde{\mathbf{y}}_u = \mathbf{W}_u^H \cdot (\tilde{\mathbf{H}}_{u,1} \mathbf{s}_1 + \dots + \tilde{\mathbf{H}}_{u,u} \mathbf{s}_u + \dots + \tilde{\mathbf{H}}_{u,K} \mathbf{s}_K + \mathbf{z}_u), \quad (20)$$

If the MU interference is perfectly cancelled by the precoder, then (20) is simplified to

$$\tilde{\mathbf{y}}_u = \mathbf{W}_u^H \cdot (\tilde{\mathbf{H}}_{u,u} \mathbf{s}_u + \mathbf{z}_u). \quad (21)$$

Therefore, using (21), the MMSE MIMO detector to the u th user is given by

$$\mathbf{W}_{MMSE,u} = \tilde{\mathbf{H}}_{u,u} \cdot \left[(\tilde{\mathbf{H}}_{u,u})^H \tilde{\mathbf{H}}_{u,u} + \frac{I_{n_{ss,u}}}{\text{SNR}_u} \right]^{-1}. \quad (22)$$

However, if the cancellation of MU interference is imperfect, the MMSE MIMO detector, using (19), is given by [11]

$$\mathbf{W}_{MMSE,u} = \tilde{\mathbf{H}}_{u,u} \cdot \left[(\tilde{\mathbf{H}}_u)^H \tilde{\mathbf{H}}_u + \frac{I_{n_{ss,u}}}{\text{SNR}_u} \right]^{-1}. \quad (23)$$

According with (22), the number of VHT-LTF to estimate the channel in the sounding procedure should be equal to the number of SSs transmitted to the u th user since the matrix $\tilde{\mathbf{H}}_{u,u}$ has size $n_{r,u}$ by $n_{ss,u}$. However, if the MMSE MIMO detector takes the MU-MIMO interference into account and the VHT-LTF uses an orthogonal Hadamard cover matrix, then (23) shows that the VHT-LTF must have a number of SSs specified

by (24), i.e., the SSs transmitted to all users must be considered in order to estimate the matrix $\tilde{\mathbf{H}}_u = \mathbf{H}_u \mathbf{P}$ with size $n_{r,u}$ by $n_{ss,total}$ [2, pp. 431], [11].

$$N_{LTF} = \begin{cases} n_{ss,total} & \text{if } n_{ss,total} = 1, 2, 4, 6, 8 \\ n_{ss,total} + 1 & \text{if } n_{ss,total} = 3, 5, 7 \end{cases} \quad (24)$$

Henceforth, we label the linear detectors that implement (23) as follows: (1) the interference cancellation MMSE (IC-MMSE) MIMO detector has more receive antennas than the number of SS transmitted to the u th STA (i.e., spatial DoF are used to improve the cancelling of MU-MIMO interference); (2) the MSSE MIMO detector has the number of receive antennas equal to the number of SS transmitted to the u th STA. Finally, note that (23) resumes to (22) for single-user (SU) MMSE MIMO detector.

III. PERFORMANCE ANALYZES

Tab. I shows the main characteristics of the IEEE 802.11ac simulator that we have been working on [12]. In this paper, we assume a BW of 80 MHz and soft-decision Viterbi decoding. The soft-decision Viterbi decoding algorithm implements the soft-output demapper for binary interleaved code modulation (BICM) proposed in [14].

Tab. II shows the IEEE 802.11ac modulation and code schemes (MCS) analyzed in this paper.

Table I– Parameters of IEEE 802.11ac simulator [12].

Parameter	Value	Parameter	Value
Carrier Frequency	5.25 GHz	MCS	0-9
Bandwidth	20 MHz, 40 MHz, 80 MHz	Number of Spatial Streams	1 to 8
GI Length	800 ns	Synchronization	Auto-Correlation
Modulation	BPSK, QPSK, 16-QAM, 64QAM, 256-QAM	MIMO Channel Estimation	Least Square
Binary Convolutional Code (BCC)	Code rate: $r=1/2, r=2/3, r=3/4, r=5/6$	Channel Decoder	Hard and Soft-Decision Viterbi Decoding

Table II - MCS investigated in this paper. The PHY data rates assume a guard-interval (GI) of 800 ns and BW of 80 MHz.

	Mod	BCC Code Rate	# SSs	Data Rate Mbps
0	BPSK	1/2	1	29.3
			2	58.5
1	QPSK	1/2	1	58.5
			2	117.0
2	QPSK	3/4	1	87.8
			2	175.5
3	16-QAM	1/2	1	117.0
			2	234.0

In the sequel, a MU-MIMO TGac channel with n_t transmit antennas, an equal number of $n_{r,u}$ receive antennas per each one of the K STAs that load the channel is denoted by $TGac [n_t, n_r, K, n_{ss}]$, where it is postulated that the same number of SS n_{ss} is transmitted for each one of the K STAs.

The simulation results consider the spatial correlated and frequency selective TGac D channel model [13]: a typical office channel with maximum excess delay of 390 ns and root

mean square (rms) delay spread of 50 ns [2, pp. 38]. The Doppler power spectrum (DPS) in the TGn MIMO channel model is modeled as follows [2, pp. 45]:

$$S_d(f) = \frac{\sqrt{A}/(\pi f_d)}{1+A\left(\frac{f}{f_d}\right)^2}, \quad |f| \leq f_{max}. \quad (25)$$

where $f_d = \frac{v}{c} f_c$ denotes the Doppler spread; f_c denotes the carrier frequency in Hz; c the speed of light and v_0 is the environmental speed (i.e., v_0 is fixed in 1.2 km/h, given $f_d \approx 6$ Hz at 5 GHz band and coherence time of 50 ms when correlation of 50% is assumed). The constant A equals to 9 means that the spectrum is 10 dB below the peak at the Doppler spread frequency.

The system default configuration assumes no compression and delay in the CSI feedback scheme; no Doppler spread and MPDU payload of 1500 octets.

A. Effects of Equivalent Channel Matrix on the Transceiver Performance

Fig. 2 compares the performance of 802.11ac transceivers with RI-MMSE precoder that uses either the "complete" \mathbf{H}_{DL} channel matrix or the "equivalent" DL MU-MIMO channel matrix given by (5). The RX implements the MMSE MIMO detector. This figure shows the MPDU packet error rate (PER) as a function of SNR over the $TGac D [4,2,2,2]$ channel. Surprisingly, for MCS0 and MCS1, the performance of RI-MMSE precoder that uses the "equivalent" DL MU-MIMO channel matrix \mathbf{H}_{EQ} presents a superior performance w.r.t. the RI-MMSE precoder that uses the "complete" \mathbf{H}_{DL} matrix (see Eq. 1). We believe that this happens because the noise increases the entropy in the CSI when the matrix of left-singular vector is transmitted in the feedback frame. However, the same performance is observed for MCS3 for both types of CSI feedback since the higher SNR decreases the noise effects in the estimated CSI.

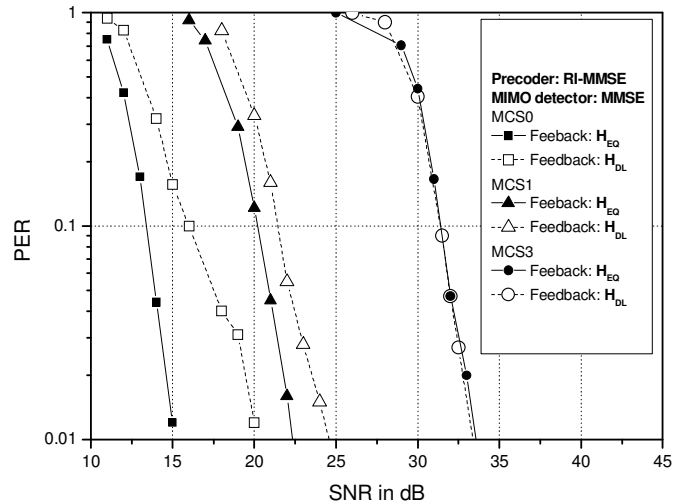


Figure 2. Effects on the PER of the CSI used to calculate the RI-MMSE precoder: $TGac D [4,2,2,2]$ channel and MMSE MIMO detector.

- **Lesson 1:** the feedback scheme specified in the IEEE 802.11ac amendment improves the performance at medium SNR regime in relation to systems that use the complete DL MU-MIMO channel matrix to calculate the precoding filter coefficients when the MMSE MIMO detector is implemented.

Fig. 3 shows results in order to compare the performance between IC-MMSE and CI-ZF (Channel Inversion-Zero Forcing) precoders, assuming $TGac D [4,2,4,1]$ and MCS2. The CI-ZF precoder is modeled by Eq. (14) with \overline{SNR} set to zero. These results also allow comparing the performance between IC-MMSE and IC-ZF MIMO detectors, where the IC-ZF spatial equalizer is given by Eq. (23) with SNR_u set to zero. Finally, Fig. 3 also investigates the 802.11ac WLAN performance when it is implemented the RI-MMSE precoder and MMSE MIMO detector (Eq. 22), assuming $TGac D [4,2,4,1]$ with MCS1.

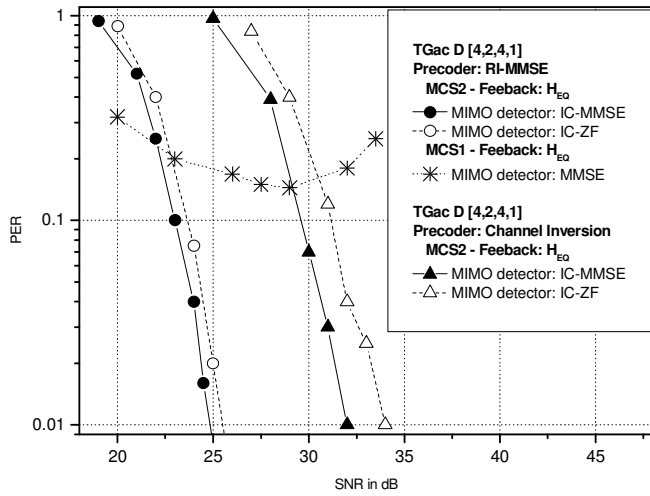


Figure 3. Comparison between the performance of RI-MMSE and CI-ZF precoders over $TGac D [4,2,2,2]$ channel with the following MIMO detectors: IC-MMSE; IC-ZF and MMSE.

- **Lesson 2:** the implementation of CI-ZF precoder entails a substantial power loss w.r.t the RI-MMSE precoder.
- **Lesson 3:** the use one degree of freedom to cancel the interference at RX side helps reduce the power losses of IC-ZF MIMO detector w.r.t. IC-MMSE MIMO detector (i.e., 0.5 and 1 dB for systems with RI-MMSE and CI-ZF precoders, respectively).
- **Lesson 4:** the implementation of MMSE (Eq. 21) instead of IC-MMSE MIMO detector (Eq. 22) causes an error floor in systems with available spatial degrees of freedom (DoF) to cancel the residual MU interference. This explains the overhead (see Eq. 24) of the DL MU-MIMO sounding procedure specified in the IEEE 802.11ac amendment [1-2],[11].

Fig. 4 shows that practically the same performance is obtained when the RI-MMSE precoder uses either the matrix H_{DL} or the matrix H_{Eo} to calculate the matrix P_{MMSE} when the receiver implements the IC-MMSE MIMO detector over the $TGac D [4,2,4,1]$ MIMO channel. Finally, observe that this figure also depicts a performance loss when the TX uses only

the matrix V (i.e., the matrix S is replaced by a unitary matrix I in Eq. 5) to calculate the RI-MMSE precoder for both configurations used at RX side, i.e., IC-MMSE and MMSE MIMO detectors.

B. Effects of Feedback Compression on the Transceiver Performance

Figures 5 and 6 allow analyzing the effects of compressed feedback on the performance of MU-MIMO transceivers with RI-MMSE precoder and the following MIMO detectors: MMSE ($TGac D [4,2,2,2]$ in Fig. 5); IC-MMSE ($TGac D [4,2,4,1]$ in Fig. 6). Notice that the number of bits necessary to avoid an expressive power loss has a strong dependence with the MIMO detector implemented and MCS used. For example, assuming a PER of 1% and MCS0, a system with MMSE MIMO detector (see Fig. 5) presents a power loss of 1 dB when b is set to 3 in (13), i.e. $(\psi, \phi) = (3,5)$ bits. However, there is a negligible power loss when the IC-MMSE MIMO detector is implemented with b equal to 3 (cf. Fig. 6). Notice that the PER can even increase with the SNR increase when the plain MMSE MIMO detector is implemented, as shown in Fig. 5 for MCS0 and MCS1, due to the increasing of multi-user interference with the quantization error in the CSI available at TX side. Finally, notice that Fig. 5 shows that the transceiver that implements RI-MMSE precoder and MMSE MIMO detector demands more bits (i.e., $b=6$) than the maximum value specified in the IEEE 802.11ac amendment (i.e., $b=4$) in order to avoid a dramatic power loss when the MCS2 is used.

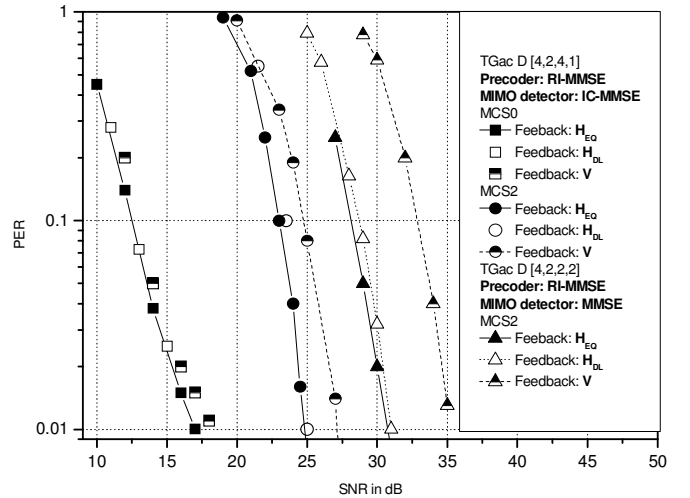


Figure 4. Effects on the PER of the CSI used to calculate the RI-MMSE precoder: $TGac D [4,2,4,1]$ channel with IC-MMSE MIMO detector and $TGac D [4,2,2,2]$ channel and MMSE MIMO detector.

- **Lesson 5:** the implementation of IC-MMSE MIMO detector at RX side decreases the power loss sensibility w.r.t the type of CSI (H_{DL} or H_{Eo}) fed back by the beamformers.
- **Lesson 6:** the precoder must use the matrix of singular values S to build the equivalent channel matrix in order to avoid a loss of performance. The power loss due to not using the matrix S increases with the modulation cardinality (i.e., MCS0=BSPK; MCS2=QPSK, as shown in Tab. 2).

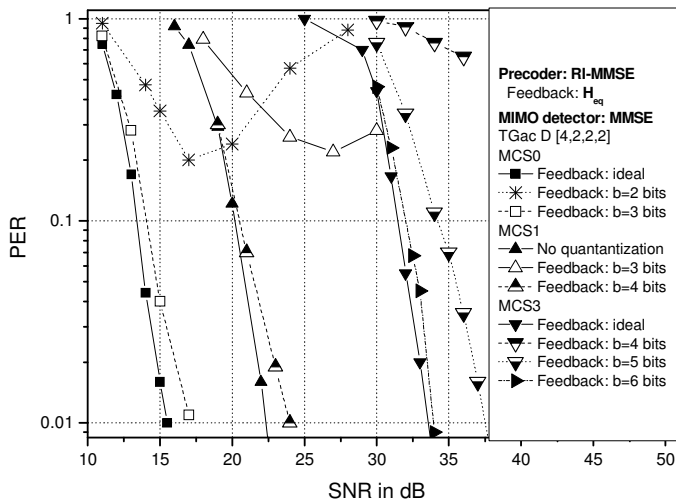


Figure 5. Effects on the PER of the feedback compression: *TGac D* [4,2,2,2] channel with MMSE MIMO detector.

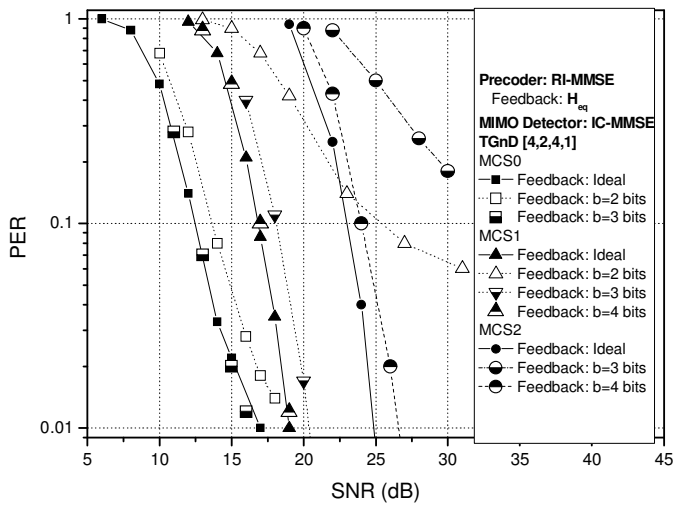


Figure 6. Effects on the PER of the feedback compression: *TGac D* [4,2,4,1] channel with IC-MMSE MIMO detector.

- **Lesson 7:** transceivers with IC-MMSE MIMO detector present lower sensibility with feedback compression w.r.t. transceivers that implement MMSE MIMO detectors.
- **Lesson 8:** the number of bits necessary to compress the information without significant power losses should be determined on the flight using smart iterative algorithms since the system performance presents a strong dependence with a multitude of variables (e.g., MIMO detector, MCS, channel characteristics and so forth).

C. Effects of Doppler Spread on the Transceiver Performance

Fig. 7 shows results that allow jointly analyzing the effects on the PER of feedback compression and delay for the following configurations: *TGac D* [4,2,2,2] channel with MMSE MIMO detector and *TGac D* [4,2,4,1] channel with IC-MMSE MIMO detector. Notice the error floor that happens with the MMSE MIMO detector when the feedback delay is set to 10 ms.

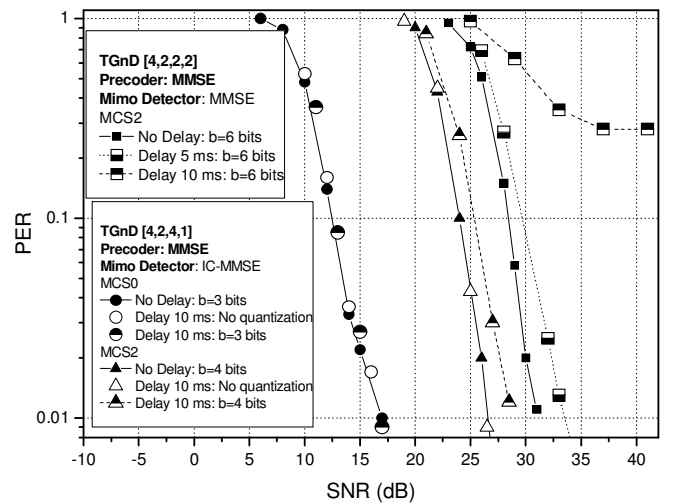


Figure 7. Effects on the PER of the feedback compression and delay: *TGac D* [4,2,2,2] channel with MMSE MIMO detector and *TGac D* [4,2,4,1] channel with IC-MMSE MIMO detector.

- **Lesson 9:** transceivers with IC-MMSE MIMO detector have a significantly lower dependence w.r.t channel sounding delay than the MMSE MIMO detector. For instance, for MCS0 a power loss of 2 dB occurs with a feedback delay of 5 ms and 10 ms for MMSE and IC-MMSE MIMO detectors, respectively.
- **Lesson 10:** the joint effects of feedback delay and compression on the performance of IC-MMSE MIMO detector have an interdependence with the MCS (e.g., no power loss for MCS0 and 2.0 dB power loss for MCS2).

D. Effects of Frequency Offset on the Transceiver Performance

The normalized frequency offset in OFDM PHY can be defined as [15, pp.27]

$$\varepsilon = \frac{\Delta f}{\Delta F}, \quad (26)$$

where Δf and ΔF denote the frequency offset and subcarriers spacing, respectively. The subcarriers spacing in the 802.11ac systems is 312.5 kHz and the maximum frequency offset is ± 232 kHz (± 20 ppm), resulting in an absolute maximum value of the normalized frequency offset given by $|\varepsilon|_{\max} \cong 0.74$.

In this paper, we implement the frequency offset estimation and residual phase tracking algorithms described and analyzed in [16].

Fig. 8 shows simulation results that take into account compression and delay of the sounding procedure, and frequency offset as well. It is shown results where the frequency offset is either equal for all STAs or assumes different values, between the minimum and maximum values specified in the IEEE 802.11ac amendment, for each STA. Notice that the performance is identical in both simulated configurations.

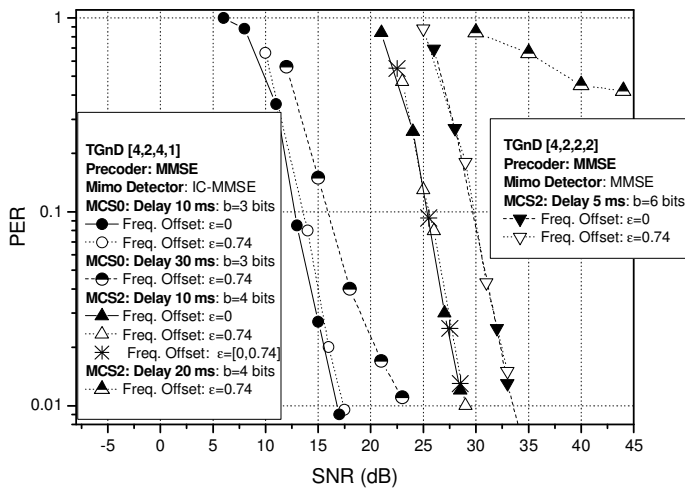


Figure 8. Effects on the PER of the frequency offset, feedback compression and delay: $TGac D [4,2,2,2]$ channel with MMSE MIMO detector and $TGac D [4,2,4,1]$ channel with IC-MMSE MIMO detector.

- **Lesson 11:** the effects of frequency offset can be mitigated by the algorithms that estimate the frequency offset using the legacy short training field (STF) and long training field (LTF), and track the residual phase using the pilots transmitted in the data field [15, 16].
- **Lesson 12:** There is a strong interdependency between the power loss, MCS and feedback delay, i.e., compare the error floor for MCS2 when the delay is set to 20 ms with the power loss for MCS0 when the delay is set to 30 ms.

IV. CONCLUSIONS

First, we described related contributions in the field of transceiver design for the DL of MU-MIMO 802.11ac WLANs, emphasizing our main contribution, i.e., a performance evaluation of transceivers with RI-MMSE precoder and IC-MMSE MIMO detector with compressed feedback over TGac MIMO channels with Doppler spread. Second, we presented in great detail the channel sounding and feedback mechanism implemented in the 802.11ac amendment, focusing on the description of Givens rotation technique used to compress the number the bits necessary to represent the equivalent channel matrix observed at RX side. After, we developed a derivation of the IC-MMSE MIMO detector and presented the IEEE 802.11ac simulator characteristics. After having established a common background, we showed a unified set of simulation results and lessons learned on the effects of CSI feedback compression and delay upon the 802.11ac DL MU-MIMO performance.

Finally, we have concluded that the effects of realistic system configuration on the performance of DL MU-MIMO transceivers depend strongly on a multitude of parameters and assumptions (channel model, number of quantization bits, MIMO detectors scheme and so forth). Therefore, we claim that developing of real time radio resource algorithms is a fundamental challenging issue to set up on the flight the system

configuration in order to balance accordingly the tradeoff between user satisfaction and system complexity.

REFERENCES

- [1] Wireless LAN Medium Access Control and Physical Layer Specifications, Amendment 5: Enhancement for Very High Throughput for Operations in Bands below 6 GHz. IEEE P802.11ac, Dec., 2013.
- [2] E. Perahia and R. Stacey, *Next Generation Wireless LANs: 802.11n and 802.11ac. 2th ed.* Cambridge: Cambridge University Press, 2013.
- [3] VK Jones and H. Sampath. "Emerging technologies for WLAN," in *IEEE Communication Magazine*, vol. 53, no. 3, pp. 141-149, March, 2015.
- [4] M. Kim and J. Kim. "Adaptive interference-aware receiver for multi-user MIMO downlink in IEEE 802.11ac," in *2015 IEEE International Conference on Consumer Electronics (ICCE)*, pp. 645-646, Las Vegas, 2015.
- [5] H. Lou, M. Ghosh, P. Xia and R. Olesen. "A comparison of implicit and explicit channel feedback methods for MU-MIMO WLAN systems," in *2013 IEEE 24th International Symposium on Personal, Indoor and Mobile Radio Communication Systems (PIMRC 2013)*, pp. 419-424, London, 2014.
- [6] W. Lin et. al. "Performance of linear precoding and user selection in IEEE 802.11ac downlink MU-MIMO system," in *2014 IEEE Wireless Communications and Networking Conference (WCNC)*, Istanbul, 2014.
- [7] J. Park et. al. "A high performance MIMO detection algorithm for DL MU-MIMO with practical errors in IEEE 802.11ac systems," in *2013 IEEE 24th Symp. on Personal, Indoor and Mobile Radio Communications*, 2013.
- [8] Y. S. Cho, J. Kim, W. Y. Yang and C. G. Kang, *MIMO-OFDM Wireless Communications with MATLAB*. Singapore: John Wiley & Sons, 2010.
- [9] R. S. Manzoor et al. "Front-end estimation of noise power and SNR in OFDM systems," in *International Conference on Intelligent and Advanced Systems 2007 (ICIAS 2007)*, Kuala Lumpur, 2007.
- [10] C. B. Peel, B. M. Howhald and A. L. Swindlehurst. "A vector - perturbation technique for near-capacity multi antenna multiuser communication - Part I: channel inversion and regularization," in *IEEE Transactions on Communications*, vol. 53, no. 1, pp. 195-202, Feb. 2005.
- [11] S. Veramani and A. V. Zelst, *Interference cancellation for downlink MU-MIMO*. IEEE 802.11-09/1234r1, 2010.
- [12] R. P. F. Hoefel. "Multi-User OFDM MIMO in IEEE 802.11ac WLAN: a simulation framework to analysis and synthesis", in *IEEE Latin America Transactions*, vol.13, no. 2, pp.540-545, Feb., 2015.
- [13] G. Breit, H. Sampath, S. Vermani, et. al., *TGac Channel Model Addendum Support Material*. IEEE 802.11-09/06/0569r0, May, 2009.
- [14] F. Tosato and P. Bisagli, "Simplified soft-output demapper for binary interleaved COFDM with applications to HIPERLAN/2," *IEEE International Conference on Communications 2002*, 2002.
- [15] R. Spitschka, *Synchronization Algorithms for OFDM Systems Using the Example of WLAN*. Saarbrücken, Germany: VDM Verlag, 2008.
- [16] R. P. F. Hoefel. "On the synchronization of IEEE 802.11n devices over frequency selective TGn channel models," *25th Annual Canadian Conference on Electrical and Computer Engineering (CCECE 2012)*, Montreal, 2012.